JOC Note
pubs.acs.org/joc

Emission Color Tuning and Deep Blue Dopant Materials Based on 1,6-Bis(*N*-phenyl-*p*-(*R*)-phenylamino)pyrene

Kyung-Ryang Wee, Hyun-Chul Ahn, Ho-Jin Son, Won-Sik Han, Ju-Eun Kim, Dae Won Cho, and Sang Ook Kang*

Department of Advanced Material Chemistry, Korea University, Sejong, Chungnam 339-700, South Korea

sangok@korea.ac.kr

Received August 19, 2009

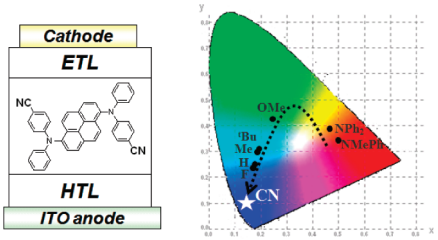

Panchromatic 1,6-bis(*N*-phenyl-*p*-(*R*)-phenylamino)pyrenes, **2R**, were obtained from Buchwald−Hartwig coupling reactions between *N*-phenyl-*p*-(*R*)-phenylamines and 1,6-dibromopyrene. The photophysical properties of **2R** corresponded well to the electron-withdrawing and -donating nature of the diarylamine substituents, exhibiting a full color visible range between 454 and 620 nm. In particular, a deep blue **2CN** showed a high radiative rate constant of 2.85×10^8 s^{-1} with high emission quantum efficiency of 79%. Further applications of **2CN** as a blue dopant were attempted using multilayer organic light-emitting devices. A maximum efficiency of 3.98 cd/A with CIE coordinates of $x = 0.14$, $y = 0.10$ were obtained.

Color control and high luminescence efficiency are fundamental issues in the development of full-color-emitting materials for organic light-emitting devices (OLEDs).[1] The establishment of a host/dopant combination at the emitting layer is indispensable in the fabrication of high performance OLEDs, and considerable effort has been made to search for the best combination. In particular, the introduction of a phosphorescent dopant has improved the electroluminescence (EL) efficiency in green and red OLEDs significantly.[2,3] However, a high performance blue phosphorescent EL is needed due to the scarcity of a suitable host/dopant energy combination.[4] Alternatively, the development of a best fluorescent host/dopant combination and subsequent device structure optimization has been a subject of current interest for the establishment of deep blue EL. Recently, a number of fluorescent blue-emitting materials, such as styrylarylene,[5] fluorene,[6] fluoranthene,[7] quinoline,[8] quinoxaline,[9] diarylanthracence,[10] triarylamines,[11] and pyrene[12] derivatives, have been reported. Among these, pyrene and its derivatives have been the subject of investigation because the absorption and emission spectra of pyrene can be tuned by systematic substitution at the 1-, 2-, 3-, 6-, 7-, and 8-positions.[13] Moreover, they exhibit high quantum efficiency[14] and high carrier mobility.[15]

SCHEME 1. Synthesis of 1,6-Bis(*N*-phenyl-*p*-(*R*)-phenylamino)-pyrenes (2R)

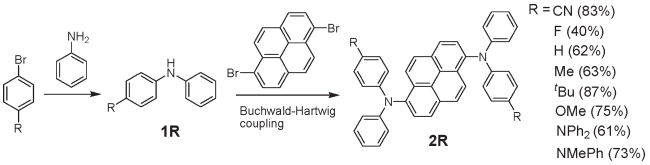

In this study, to obtain efficient deep blue pyrenes, systematic electronic variation was attempted initially by placing electron-withdrawing (EW) and -donating (ED) groups at the 4-position of bromobenzene (see Scheme 1). Further for the synthesis of para-substituted *N*-phenyl-*p*-(*R*)-phenylamine, **1R**, aniline, and 4-bromo-1-(*R*)-benzenes were coupled using a literature protocol.[16] Finally, a series of

(1) (a) Burroughes, J. H.; Bradley, D. D. C.; Brown, A. R.; Marks, R. N.; Mackay, K.; Friend, R. H.; Burns, P. L.; Homes, A. B. *Nature* **1990**, *347*, 539. (b) Tang, C. W.; VanSlyke, S. A. *Appl. Phys. Lett.* **1987**, *51*, 913.
(2) Adachi, C.; Baldo, M. A.; Thompson, M. E.; Forrest, S. R. *J. Appl. Phys.* **2001**, *90*, 5048.
(3) Su, Y.-J.; Huang, H.-L.; Li, C.-L.; Chien, C.-H.; Tao, Y.-T.; Chou, P.-T.; Datta, S.; Liu, R.-S. *Adv. Mater.* **2003**, *15*, 884.
(4) (a) Ren, X.; Li, J.; Holmes, R. J.; Djurovich, P. I.; Forrest, S. R.; Thompson, M. E. *Chem. Mater.* **2004**, *16*, 4743. (b) Chang, C.-F.; Cheng, Y.-M.; Chi, Y.; Chiu, Y.-C.; Lin, C.-C.; Lee, G.-H.; Chou, P.-T.; Chen, C.-C.; Chang, C.-H.; Wu, C.-C. *Angew. Chem., Int. Ed.* **2008**, *47*, 4542.
(5) (a) Lee, M.-T.; Liao, C.-H.; Tsai, C.-H.; Chen, C. H. *Adv. Mater.* **2005**, *17*, 2493. (b) Duan, Y.; Zhao, Y.; Chen, P.; Li, J.; Liu, S.; He, F.; Ma, Y. *Appl. Phys. Lett.* **2006**, *88*, 263503.
(6) (a) Chao, T.-C.; Lin, Y.-T.; Yang, C.-Y.; Hung, T. S.; Chou, H.-C.; Wu, C.-C.; Wong, K.-T. *Adv. Mater.* **2005**, *17*, 992. (b) Wong, K. T.; Chen, R. T.; Fang, F. C.; Wu, C. C.; Lin, Y. T. *Org. Lett.* **2005**, *7*, 1979. (c) Shen, J. Y.; Lee, C. Y.; Huang, T. H.; Lin, J. T.; Tao, Y. T.; Chien, C. H.; Tsai, C. *J. Mater. Chem.* **2005**, *15*, 2455.
(7) Chiechi, R. C.; Tseng, R. J.; Marchioni, F.; Yang, Y.; Wudl, F. *Adv. Mater.* **2006**, *18*, 325.
(8) Tonzola, C. J.; Kukarni, A. P.; Gifford, A. P.; Kaminsky, W.; Jenekhe, S. A. *Adv. Funct. Mater.* **2007**, *17*, 863.
(9) (a) Chen, C.-T.; Wei, Y.; Lin, J.-S.; Moturu, M. V. R. K.; Chao, W.-S.; Tao, Y.-T.; Chien, C.-H. *J. Am. Chem. Soc.* **2006**, *128*, 10992. (b) Wei, Y.; Samori, S.; Tojo, S.; Fujitsuka, M.; Lin, J.-S.; Chen, C.-T.; Majima, T. *J. Am. Chem. Soc.* **2009**, *131*, 6698.
(10) Kim, Y. H.; Jeong, H. C.; Kim, S. H.; Yang, K.; Kwon, S. K. *Adv. Funct. Mater.* **2005**, *15*, 1799.
(11) Liu, Q. D.; Lu, J.; Ding, J.; Day, M.; Tao, Y.; Barrios, P.; Stupak, J.; Chan, K.; Li, J.; Chi, Y. *Adv. Funct. Mater.* **2007**, *17*, 1028.
(12) (a) Tao, S.; Peng, Z.; Zhang, X.; Wang, P.; Lee, C.-S.; Lee, S.-T. *Adv. Funct. Mater.* **2005**, *15*, 1716. (b) Mikroyannidis, J. A.; Fenenko, L.; Adachi, C. *J. Phys. Chem. B* **2006**, *110*, 20317. (c) Moorthy, J. N.; Natarajan, P.; Venkatakrishnan, P.; Huang, D.-F.; Chow, T. J. *Org. Lett.* **2007**, *9*, 5215. (d) Liu, F.; Tang, C.; Chen, Q.-Q.; Shi, F.-F.; Wu, H.-B.; Xie, L.-H.; Peng, B.; Wei, W.; Cao, Y.; Huang, W. *J. Phys. Chem. C* **2009**, *113*, 4641.
(13) (a) Rausch, D.; Lambert, C. *Org. Lett.* **2006**, *8*, 5037. (b) Kim, H. M.; Lee, Y. O.; Lim, C. S.; Kim, J. S.; Cho, B. R. *J. Org. Chem.* **2008**, *73*, 5127.
(14) Bevilacqua, P. C.; Kierzek, R.; Johnson, K. A.; Turner, D. H. *Science* **1992**, *258*, 1355.
(15) Tang, C.; Liu, F.; Xia, Y.-J.; Xie, L.-H.; Wei, A.; Li, S.-B.; Fan, Q.-L.; Huang, W. *J. Mater. Chem.* **2006**, *16*, 4074.
(16) Hartwig, J. F. *Angew. Chem., Int. Ed.* **1998**, *37*, 2046.

Published on Web 10/07/2009 DOI: 10.1021/jo901783a

TABLE 1. Photophysical Properties of 2R Measured in CH_2Cl_2

pyrenes	λ_{abs}[a] [ε][b]	λ_{em}[a] [fwhm]	Φ_f[c]	τ_F (ns)	k_{rad}[d] $\times 10^8$ s^{-1}	k_{nr}[d] $\times 10^7$ s^{-1}	k_{rad}/k_{nr}
2CN	407 nm (25333)	454 nm (46)	0.79	2.7	2.85	7.34	3.88
2F	423 nm (22233)	470 nm (56)	0.80	5.5	1.44	3.58	4.02
2H	423 nm (24833)	472 nm (55)	0.78	5.1	1.52	4.14	3.67
2Me	428 nm (25166)	484 nm (63)	0.74	6.2	1.20	4.15	2.89
2′Bu	428 nm (25466)	481 nm (62)	0.71	6.2	1.15	4.68	2.46
2OMe	432 nm (25166)	513 nm (84)	0.46	9.0	0.52	5.91	0.88
2NPh$_2$	438 nm (22800)	600 nm (121)	0.13	2.7	0.48	31.8	0.15
2NMePh	435 nm (23966)	620 nm (133)	0.01	1.1	0.17	90.9	0.02

[a]In CH_2Cl_2. [b]Molar extinction coefficient (ε, M^{-1} cm^{-1}). [c]Relative to 9,10-diphenylanthracene or rhodamine B as standards in CH_2Cl_2 at room temperature. [d]Values of k_{rad} and k_{nr} were calculated according to the equations, $k_{rad} = \Phi_f/\tau_F$ and $k_{nr} = (1/\tau_F) - k_{rad}$.

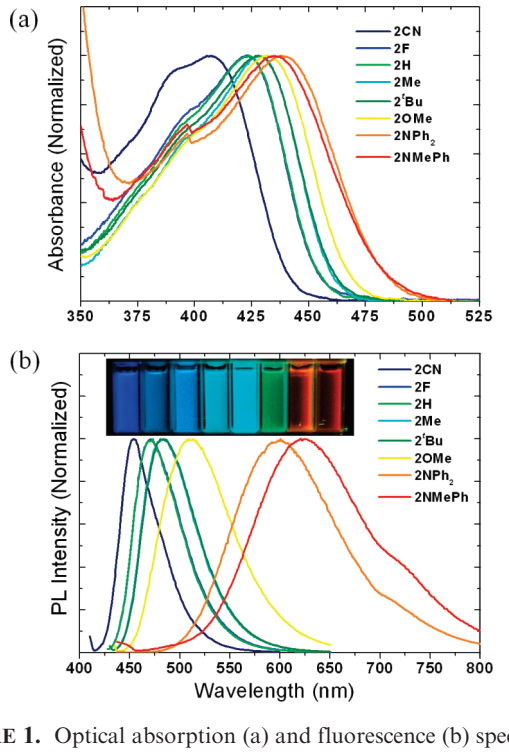

FIGURE 1. Optical absorption (a) and fluorescence (b) spectra of **2R** in CH_2Cl_2.

panchromatic 1,6-bis(*N*-phenyl-*p*-(*R*)-phenylamino)pyrenes, **2R**, where R was varied from CN, F, H, Me, ^{t}Bu, OMe, NPh_2, to NMePh, were obtained by Buchwald−Hartwig cross-coupling by reacting 2 equiv of **1R** with 1,6-dibromopyrene. The details of this synthesis are given in the Supporting Information (SI). All **2R** compounds were isolated by flash column chromatography with yields ranging from 40 to 87%, and their compositions were confirmed based on elemental and high resolution mass analyses. The structures were authenticated based on functional group analysis of the ^{1}H and ^{13}C NMR spectra, as shown in Figures S1 and S2 in the Supporting Information.

The UV−visible absorption and fluorescence spectra were measured in dichloromethane, and the spectral parameters are summarized in Table 1. As shown in Figure 1a, the absorption maxima of **2R** lie in the range of 407−435 nm due to the $\pi-\pi^*$ transition of pyrene. The spectral shifts correspond well to the electronic perturbation by the R group. The emission maxima of **2R** ranged from 454 to 620 nm (Figure 1b), and the emission profiles covered almost the entire visible light spectrum from blue to red. **2CN**, **2F**, **2H**, **2Me**, and **2′Bu** showed blue fluorescence at approximately 454−481 nm with higher PL quantum efficiency in the 71−80% range. In the case of **2NPh$_2$** and **2NMePh**, large red-shifted fluorescence emissions were observed at 600 and 620 nm, respectively. Red fluorescent materials, **2NMePh** and **2NPh$_2$**, had lower quantum yields consistent with the energy gap law[17] and are listed in Table 1.

It should be noted that the energy gap law, fluorescence quantum yields, and decay time constants are affected by the energy gap between the HOMO and LUMO.[18] Therefore, the fluorescence lifetimes (τ_F) of **2R** were measured by a time correlated single photon counting spectrometer. Using the relationship between fluorescence lifetimes and quantum yields, the radiative decay constants (k_{rad}) of **2R** were determined in the order of 10^7-10^8, notably larger than that of pyrene ($\sim 10^6$).[19] The radiationless rate constant, k_{nr}, and k_{rad}/k_{nr} of **2R** were also calculated and are listed in Table 1. The k_{rad}/k_{nr} values increased gradually with increasing electron-withdrawing power of **2R** (Table 1 and Figure S5 in SI). There was a general trend in the series. The electron-withdrawing substituents exhibited superior emissive properties, as found for **2CN** and **2F** based on the quantum yields and k_{rad}/k_{nr} value.

The electrochemical properties of **2R** were estimated by cyclic voltammetry (CV), as shown in Figure 2b and Figure S6 in SI. A positive change in the oxidation potentials from 0.21 to 0.64 V was observed from **2NMePh** to **2CN** with the highest value observed for **2CN**. From the first oxidation, the HOMO energy levels of **2R** were estimated to be ca. −4.81 to −5.31 eV, as listed in Table S1 in the SI. However, no distinct cathodic reduction process of **2R** was recorded when the electrode potential was swept continuously between 0.0 and

(17) Englman, R.; Jortner, J. *Mol. Phys.* **1970**, *18*, 145.
(18) (a) Pohl, R.; Anzenbacher, P. *Org. Lett.* **2003**, *5*, 2769. (b) Montes, V. A.; Li, G.; Pohl, R.; Shinar, J.; Anzenbacher, P. *Adv. Mater.* **2004**, *16*, 2001. (c) Bolvar, C. P.; Montes, V. A.; Anzenbacher, P. *Inorg. Chem.* **2006**, *45*, 9610.
(19) Karpovich, D. S.; Blanchard, G. J. *J. Phys. Chem.* **1995**, *99*, 3951.

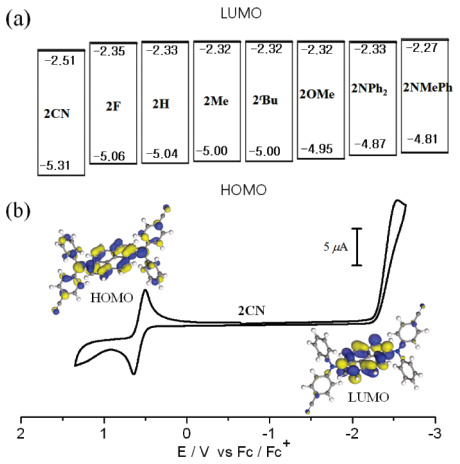

FIGURE 2. (a) HOMO−LUMO levels of **2R** obtained from the CV and absorption data. (b) CV plot of **2CN** in CH_2Cl_2 with Bu_4NClO_4 (0.1 M) as the supporting electrolyte.

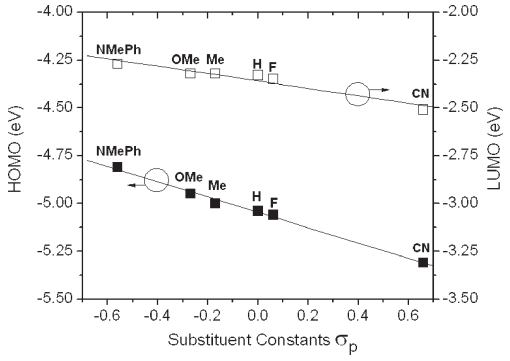

FIGURE 3. Plots of HOMO (■) and LUMO (□) levels versus Hammett substituent constants (σ_p).

−2.5 V with the exception of **2CN**. The LUMO energy levels were estimated to be −2.27 ∼ −2.51 eV from the absorption edge of the optical absorption spectra of **2R**. The HOMO levels increased with increasing electron-donating power of the R groups to a maximum difference of 0.5 eV, whereas the LUMO levels were less sensitive to electronic variations by only ∼0.24 eV (Figure 2a).

In order to better understand the key factors responsible for the differences observed in the photophysical and electrochemical properties, quantum chemical calculations for **2R** were carried out using DFT, as implemented in the Dmol^3 package.[20] As shown in Figure 2a, the electron density of the HOMO is delocalized at the peripheral diarylamines, whereas that of the LUMO is concentrated at the pyrene core. On the basis of the CV and computational data, the peripheral R groups of amines control the HOMO effectively, thereby altering the band gap. Figure 3 shows a plot of the HOMO and LUMO level as a function of the Hammett substituent constants (σ_p),[21] which correlates well with the electron-donating or -withdrawing power of the para-substituents of diarylamines. The HOMO and LUMO energy levels changed according to the σ_p values with a good linear correlation. The HOMO slope was larger than that of the

(20) (a) Delley, B. *J. Chem. Phys.* **1990**, *92*, 508. (b) Delley, B. *J. Chem. Phys.* **2000**, *113*, 7756.
(21) Hansch, C.; Leo, A.; Taft, R. W. *Chem. Rev.* **1991**, *91*, 165.

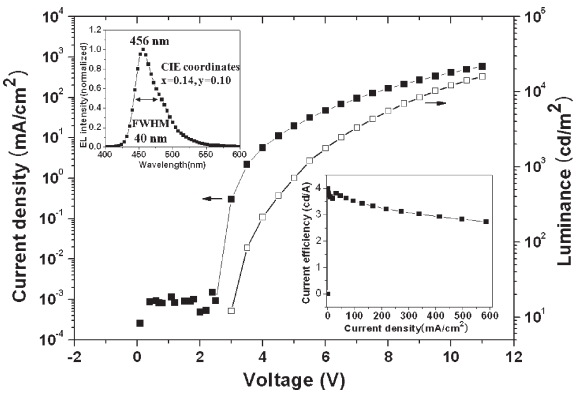

FIGURE 4. The $I-V-L$ curve of the **2CN** device (ITO/DNTPD/NPD/ADN:**2CN**(11%)/PyPySPyPy/LiF/Al). The insets denote the current efficiency and EL spectrum.

TABLE 2. EL Performance of 2CN Dopant with Various Doping Ratio at 20 mA/cm^2

dop (%)	V_{on} [a]	V	L [b]	η_{ex} [c]	η_{lum} [d]	η_{pw} [e]	L_{max} [f]	CIE (x, y)
0	3	5.7	200	1.1	1.00	0.60	4459	0.15, 0.11
5	3	5.1	620	3.7	3.10	1.90	15460	0.14, 0.10
7	3	5.2	636	3.7	3.18	1.90	12880	0.14, 0.10
9	3	5.0	710	4.1	3.55	2.23	16140	0.14, 0.10
11	3	5.0	728	4.0	3.64	2.49	16030	0.14, 0.10

[a]Turn-on voltage (V). [b]Luminance (cd/m^2). [c]External quantum efficiency (%). [d]Luminance efficiency (cd/A). [e]Power efficiency (lm/W). [f]Maximum luminance (cd/m^2).

LUMO with respect to σ_p. These results clearly show that the spectral shift in absorption and PL was attributed to a decrease in the HOMO levels rather than a decrease in the LUMO levels.

The potential application of **2CN** as a blue dopant was evaluated by fabricating OLED devices with various doping ratios and the following configuration: ITO/DNTPD (65 nm)/NPD (20 nm)/ADN: **2CN** (0, 5, 7, 9, 11%) (35 nm)/PyPySPyPy (20 nm)/LiF (1 nm)/Al (100 nm), where ITO (indium tin oxide) was the anode, DNTPD (*N*,*N*′-[*p*-di(*m*-tolyl)aminophenyl]-*N*,*N*′-diphenylbenzidine) served as a hole-injection layer, NPD (*N*,*N*′-bis(naphthalen-1-yl)-*N*,*N*′-bis(phenyl)benzidine) as a hole-transporting layer, ADN (9,10-di(2-naphthyl)anthracene) and **2CN** as emitting layer, PyPySPyPy (2,5-bis(2′,2″-bipyridin-6-yl)-1,1-dimethyl-3,4-diphenylsilacyclopentadiene) as an electron-transporting layer, and LiF:Al as the composite cathode. Figure 4 and Figure S7 in SI show the current−voltage−luminance ($I-V-L$) characteristics of the **2CN** devices, and their device characteristics at 20 mA/cm^2 are listed in Table 2.

The EL spectrum for the **2CN** devices was featureless with the maximum peak at 456 nm with CIE coordinates of x = 0.14 and y = 0.10. The similarity of the photoluminescence (PL) and EL spectra suggests that the EL was attributed to emission from the radiation decay of the excited singlet state of **2CN**. The EL efficiency increased slightly when the **2CN** concentration was increased from 5 to 11%, as shown in Table 2.

As shown in Figure 4, the 11% doped **2CN** device showed promising performance compared with previous pyrene-based devices,[11] exhibiting a turn-on potential of 3.0 V and a maximum brightness of 16030 cd/m^2 at 586 mA/cm^2 (11 V), as well as maximum current and power efficiencies

of up to 3.98 cd/A and 4.17 lm/W, respectively. Moreover, the efficiency of the device showed no significant fall off from a low current density to a higher current density.

In summary, a series of 1,6-bis(*N*-phenyl-*p*-(*R*)-phenylamino)pyrenes, **2R**, were prepared using a Buchwald−Hartwig coupling reaction. The emission colors were controlled by introducing electron-donating or -withdrawing R groups. The OLED device based on **2CN** as a dopant showed a maximum efficiency of 3.98 cd/A with CIE coordinates of $x = 0.14$ and $y = 0.10$. These results suggest that the **2CN** is a promising blue-emitting material for the preparation of highly efficient deep blue devices. Further studies focusing on additional structural tuning of the **2R** series with the aim of improving its color purity and quantum efficiency as well as device optimization are currently underway.

Experimental Section

Compound 2CN. 1,6-Dibromopyrene (1.00 g, 2.78 mmol), 4-(phenylamino)benzonitrile (1.19 g, 6.12 mmol), $Pd_2(dba)_3$ (0.127 g, 5 mol %), and NaO^{t}Bu (1.92 g, 20 mmol) were added to a mixture of toluene (60 mL). The resulting mixture was stirred under N_2 at 110 °C for 12 h. The mixture was hydrolyzed with water. The organic layer was extracted with CH_2Cl_2 (3 × 30 mL) and dried over magnesium sulfate. The solvent was removed under reduced pressure, and the residue was purified by silica gel column chromatography using CH_2Cl_2/hexane (1:4) as the eluent. **2CN** was obtained as a pale yellow powder (1.35 g, 83%) and further purified by train sublimation in 67% yield: ^{1}H NMR ($CDCl_3$) δ 8.18 (d, 2H), 8.08 (d, 2H), 7.99 (d, 2H), 7.85 (d, 2H), 7.39 (d, 4H), 7.30 (t, 4H), 7.24 (d, 4H), 7.13 (t, 2H), 6.88 (d, 4H); ^{13}C NMR ($CDCl_3$) δ 152.4, 146.4, 139.6, 132.6, 130.4, 130.0, 128.7, 128.5, 128.3, 127.0, 126.5, 125.1, 123.1, 119.9, 118.7, 102.5; HRMS(FAB) calcd for $C_{42}H_{26}N_4$ 586.2157, found 586.2112 [M]+. Anal. Calcd for $C_{42}H_{26}N_4$: C, 85.98; H, 4.47; N, 9.55. Found: C, 85.92; H, 4.41; N, 9.49.

Acknowledgment. This work was supported by the National Research Foundation of Korea (NRF) grant funded by the Korea government (MEST) (No. 2009-0083181) and ERC Program (No. 2009-0063377).

Supporting Information Available: Experimental details and characterization data (^{1}H, ^{13}C NMR), CVs, *I*−*V*−*L* characteristics of OLEDs, and calculation data. This material is available free of charge via the Internet at http://pubs.acs.org.